We are IntechOpen,
the world's leading publisher of
Open Access books
Built by scientists, for scientists

6,900
Open access books available

186,000
International authors and editors

200M
Downloads

Our authors are among the

154
Countries delivered to

TOP 1%
most cited scientists

12.2%
Contributors from top 500 universities

CLARIVATE ANALYTICS
BOOK CITATION INDEX
INDEXED

WEB OF SCIENCE™

Selection of our books indexed in the Book Citation Index
in Web of Science™ Core Collection (BKCI)

Interested in publishing with us?
Contact book.department@intechopen.com

Numbers displayed above are based on latest data collected.
For more information visit www.intechopen.com

WMR Kinematic Control Using Underactuated Mechanisms for Goal Direction and Evasion

Jorge U. Reyes-Muñoz, Edgar A. Martínez-García,
Ricardo Rodríguez-Jorge and Rafael Torres-Córdoba

Additional information is available at the end of the chapter

Abstract

This work presents the mechanical design and the kinematic navigation control system for a tricycle-wheeled robot (one drive-steer and two lateral fixed passive) with two underactuated mechanisms: a global compass and local evasive compass. The proposed goal-reference mechanism is inspired by the ancient Chinese south-seeking chariot (c. 200–265 CE) used as a navigation compass. The passive lateral wheels transmit an absolute angle from its differential speeds to automatically steer the front wheel. An obstacle-evasive compass mechanism is commutated for steering control when detecting nearby obstacles. The absolute and local compass mechanisms commutate each other to control to the robot's steering wheel to reach a goal while avoiding collisions. A kinematic control law is described in terms of the robot's geometric constraints and is combined with a set of first-order partial derivatives that allows interaction between the global and local steering mechanisms. Animated simulations and numerical computations about the robot's mechanisms and trajectories in multi-obstacle scenarios validate the proposed kinematic control system and its feasibility.

Keywords: WMR, kinematic control, south-seeking chariot, underactuated compass, potential-field, self-steer, navigation

1. Introduction

So far today, numerous types of modern robotic platforms that perform complex tasks are composed of underactuated mechanisms that were deployed by ancient civilizations. Underactuated mechanisms prevail as the most efficient systems because they take more advantage applying the law of conservation of energy than redundantly kinematic systems. Unlike redundant systems, the underactuated systems pose a reduced number of actuators and less independent control variables and naturally take more advantage of the inertial and gravity forces. The redundant systems have a larger number of control variables than variables in the working

space. As a consequence, each controlled actuator somehow has to counteract gravity and inertial forces to establish own kinematic behaviors. A major aspect in robotics engineering concerns physical modeling and control of mobility for a robot to provide autonomous navigation. Similar to any biological entity, the ability to purposely navigate is fundamental for an intelligent robot. Over 2000 years ago, the Chinese invented the south-seeking chariot (SSC), which was used to maintain an absolute orientation along very long trips of hundreds of kilometers. Thus, they basically created one of the first absolute direction compass devices that did not require any other element to function, but its inner mechanisms only. The invention's compass was used to adjust toward a desired orientation at the beginning of a trip, and it was invented nearly 800 years in advance when the magnetic compass was invented. The SSC is basically a differential gearing system with a pointing-out silhouette above (**Figure 1**). The gearing system compensates the chariot turns by gear transmission relations, keeping the statue arm pointing out always to the same direction. **Figure 1a** shows the SSC design, and **Figure 1b** depicts the SSC prototype with its gearing system made of straight wooden gears. However, this system has largely been studied in modern times by numerous authors [1–7].

Any type of navigational and path-tracking task depends on steering systems. And, in order to infer navigation references, mobile robots use a diversity of exteroceptive sensing devices, such as ultrasound sonar, infrared range detectors, cameras, GPS, and so forth. Nevertheless, a common disadvantage using these types of devices is that they have to obtain external measurements with respect to (w.r.t.) the robot's fixed Cartesian coordinate system and use them to estimate orientation through geometry models with cumulative errors.

Moreover, some types of proprioceptive sensing devices offer inner measurements that are relative to global inertial system (e.g., magnetic compass, GPS). Unlike local exteroceptive sensors, global proprioceptive sensors yield noncumulative overtime measurement errors. For instance, a magnetic compass implemented as a global orientation system measures angle w.r.t. the earth magnetic axis. And then, such measurement angle is arithmetically used to infer a global destination angle likely described in another external inertial system. However, magnetic compasses are sensitive and are affected by other nearby magnetic fields or tided to suffer errors from rotations that set the device perpendicular to the earth's magnetic axis. Therefore, other

(a)   (b)
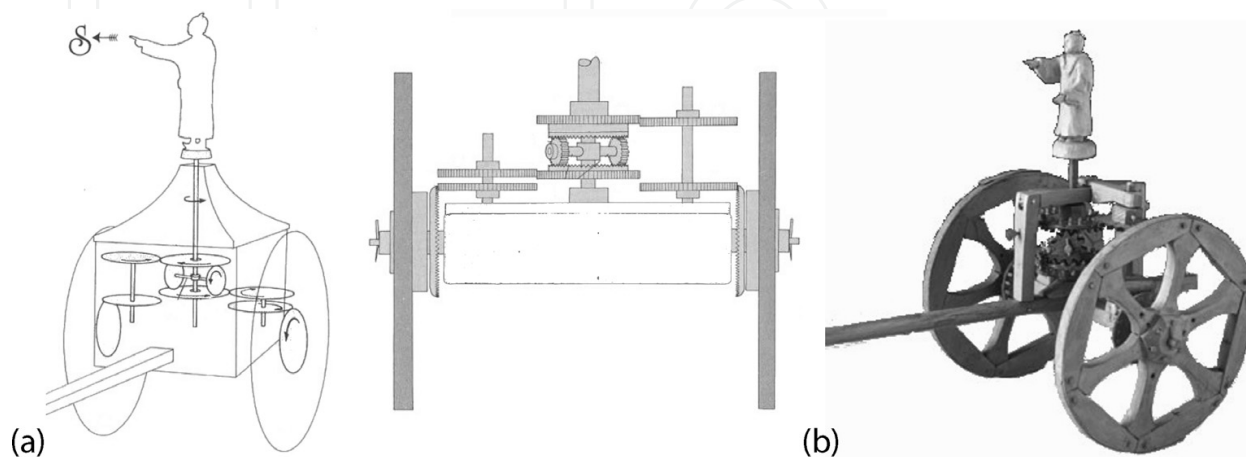
Figure 1. South-pointing chariot. (a) Modern design and (b) modern prototype.

types of sensing devices must be combined to recover from missed observations. Furthermore, the global positioning system (GPS) is another type of global orientation measurement device, which requires at least two successive position observations overtime to provide an instantaneous robot's global angle w.r.t. the earth's geographic north pole. As a major disadvantage, GPS cannot provide measurements nearly of inside buildings, forests, or in cloudy days because electromagnetic signals are blocked missing observations during arbitrary periods of time.

A diversity of works has reported navigation systems that combine numerous types of measuring orientation devices such as GPS and magnetic compasses, which provide high precision. This type of technology produces sensing measurements tided to established references (e.g., magnetic/north pole). Hence, useful global-specific references have to be inferred by different methods, which may imply in these calculations inverse/direct solutions of geometric triangulations or algebraic models [8–12].

Reliable local/global navigation for a wheeled mobile robot has fundamentals on controllability and maneuverability. And, both robot's abilities, respectively, must depend on robust driving control models and the steering kinematic designs [13, 14]. These models are the bases for planning and motion control [15, 16] in navigation, and most of them relay on different numerical mathematical solutions in robotics [17]. There are some complex works on robot's navigation seeking absolute orientation references [19, 20]. There are other navigation works with major emphasis on collision avoidance relaying on kinematic approaches [18, 21].

In this work, the mechanical design, the physical model, and a control system for a tricycle-wheeled robot with fundamentals on underactuated mechanical functions are proposed. The self-steer robot design proposed in this work has been inspired on the south-seeking chariot, in part, to take advantage of the underactuated mechanical compass with absolute direction to the robot's goal. Therefore, a specific and complex gearing mechanism system was designed to self-steer commuting between an obstacle-avoiding compass and a leading-to-the-goal compass (**Figure 2**).
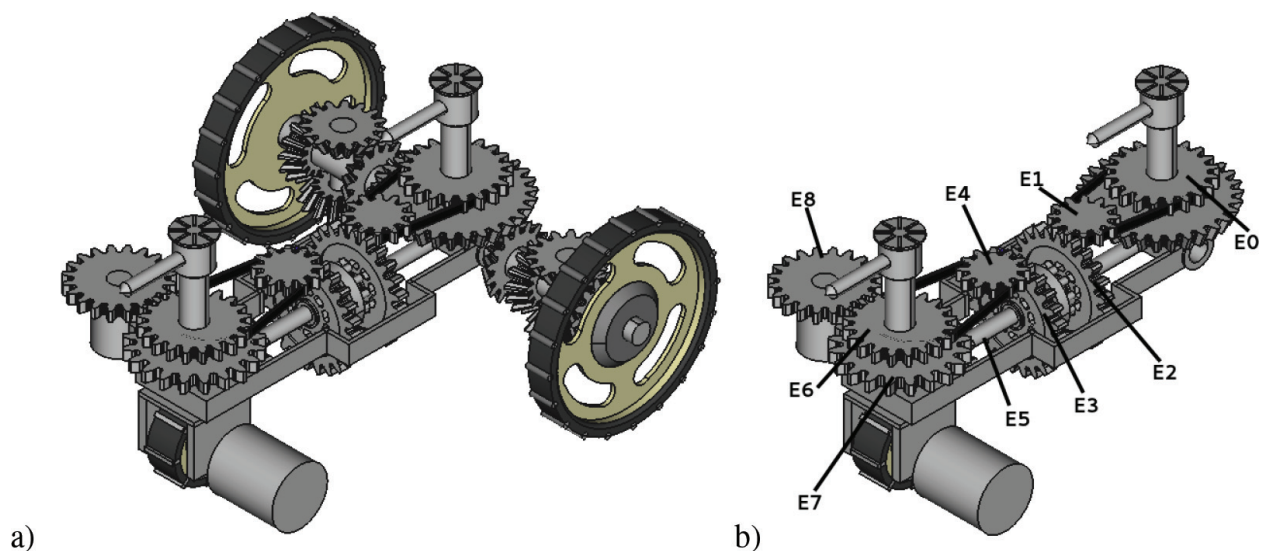
Figure 2. Proposed tricycle robot system. (a) General system view and (b) absolute/local compass mechanism.

The global goal-reference compass permanently maintains orientation information available in a direct manner for the robot without sensors, despite experimenting multiple evasive maneuvers.

A kinematic model for the local/global compass and commutation mechanisms are deduced. Moreover, a kinematic control law deduced for a three-wheeled structure with one drive-steer frontal wheel and a pair of lateral passive wheels is analyzed and disclosed. The proposed control law estimates the robot's posture and combines the interactive switching between goal-leading and obstacle avoidance navigation control. One underactuated mechanism directly leads the robot to the goal. Another underactuated mechanism leads the robot toward free-collision routes.

This manuscript presents simulation results to validate this novel approach that combines ancient underactuated automaton type, with a modern-wheeled robot focus. So far today, the authors are not conscious about other similar approaches reported in the scientific literature. This work does not pretend to introduce a comparative analysis nor efficiency with other state-of-the-art robotic trends. The authors of this research believe that the preliminary results presented in this manuscript will evolve into an efficient technological approach in the near future. Its application will establish a novel approach because it allows to directly have absolute angle observation overtime, allowing the mechanisms to lead the robot with naturally global navigation, reducing computational efforts to other algorithmic tasks, and complementing other sensing devices to improve control and perception.

Sections of this chapter have been organized in the following manner. Chapter 2 discloses the kinematic models for the absolute/local mechanisms. In Chapter 3, the commutation system kinematic and time delays are discussed. In Chapter 4, the control model and simulation results are presented. Finally, Chapter 5 discusses some conclusive remarks about this work.
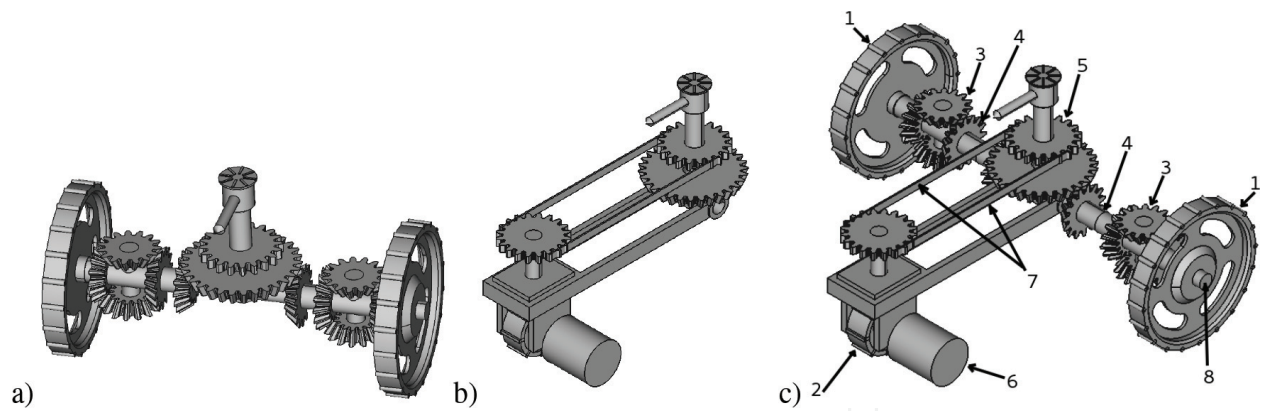
2. Absolute/local compass mechanism

### 2.1. Global underactuated compass

The proposed system sets the robot's desired Cartesian goal as the absolute reference orientation. The absolute compass directly compensates its bearing by the differential angle provided by the two lateral wheels (**Figure 3a**). The mechanical compass directly self-steer the robot toward the global reference without any actuator (**Figure 3b**). When the robot is not leading along the global compass angle, the synchronization chain gradually reorientates the robot's steering wheel until matching the goal's absolute angle. **Figure 3c** illustrates the self-steering mechanism parts: (1) passive lateral wheels, (2) frontal driving wheel with passive steering, (3) wheel differential gearing mechanisms, (4) transmission gears coupling the absolute compass, (5) global goal-angle compass, (6) driving actuator/motor, (7) self-steer synchronization chain, and (8) lateral wheel shaft.

In **Figure 4**, a more detailed depiction of the differential mechanism is illustrated. The absolute compass (5) is composed of three differential systems (3) and (5), which transmit rotary motion from the lateral wheels (1) up to the steering wheel (2) (see **Figure 4b**). The compass (5) is

Figure 3. Absolute compass system. (a) Wheel differential mechanisms, (b) self-steer mechanism, and (c) goal-reference self-steer robot mechanism.
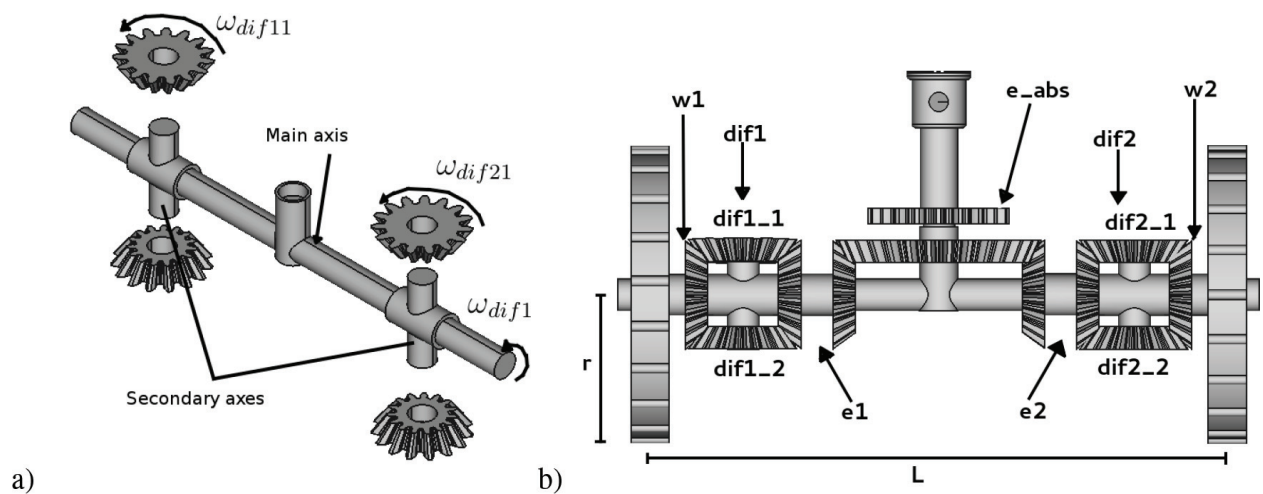
Figure 4. Differential gearing system. a) wheel main shafts, b) absolute direction differential.

compensated by the gearing relations (**Figure 4b**), and the differential rotary motion is transmitted to the gear (5), namely, e_{abs}. It is worth noting that the differential motion (3) of the lateral wheels' shaft (8) is fixed to the main axis (4). The lateral wheels' angular speeds, dubbed w_1 and w_2, are asynchronous w.r.t. the main shaft (4), similarly differential gears e_1 and e_2. The differential shafts of gears dif_1 and dif_2 (**Figure 4b**) are perpendicularly joined to the main axis (**Figure 4a**), and the rotary speed is basically the same for both differentials (4). Nevertheless, the angular velocity for gears ($dif1_1$, $dif1_2$, $dif2_1$, and $dif2_2$) might be different for each differential mechanism (3); it would depend on each wheel's (1) instantaneous velocity.

Finally, the compass, differential mechanism (5) that is composed of the gears e_1, e_2, and e_{abs} is the mechanism providing the absolute orientation reference toward the robot's goal.

Without loss of generality, it follows that the deduction of the differential angular velocity model transmitted between e_1 and e_2 is provided next. Thus, the angular velocity for ω_{e1} is an averaged differential value:

$$\omega_{e1} = -\frac{\omega_1 - \omega_2}{2} \tag{1}$$

where both lateral angular speeds have clockwise (left-sided wheel) and counterclockwise (right-sided wheel) signs, respectively:

$$\omega_{e1} = -\omega_{e2} \tag{2}$$

The differential angular speed is equivalent to the main shaft rotary speed, such that

$$\omega_{dif1} = \omega_{dif2} = \frac{\omega_1 - \omega_2}{2} \tag{3}$$

and, in general, it is assumed that the gears' ($dif1$ and $dif2$) angular velocities are averaged values:

$$\omega_{dif11} = \omega_{dif12} = \frac{\omega_1 + \omega_{e1}}{2} \tag{4}$$

as well as

$$\omega_{dif21} = \omega_{dif22} = \frac{\omega_2 + \omega_{e2}}{2}. \tag{5}$$

In such a manner, the angular velocity transmitted to the compass e_abs poses the following relation:

$$\omega_{e_{abs}} = \frac{r_{e_{abs}}}{r_{e_1}} \omega_{e1}, \tag{6}$$

In the proposed design, it is assumed that the gear e_abs doubles its radius w.r.t. gears e_1 and e_2. Therefore, by rewriting Eq. (6)

$$\omega_{e_{abs}} = \frac{1}{2} \omega_{e1}, \tag{7}$$

and by substituting in the previous expression, the differential rotary speed model ω_{e1} since ultimately depends on velocities ω_1 and ω_2:

$$\omega_{e_{abs}} = -\frac{\omega_1 - \omega_2}{4}. \tag{8}$$

Therefore, from the previous expression, let us assume that the robot moves along a straight trajectory line, then $\omega_1 = \omega_2$, and no compass lateral motion is yielded; hence, $\omega_{e_{abs}} = 0$. Following **Figure 2b** notation for the gears, the steering wheel with gear E_7 is synchronized with $\omega_{e_{abs}}$ by the mechanism system illustrated in **Figure 5a**.

A first gear connection $E0 - E1$ has the following speed relation:
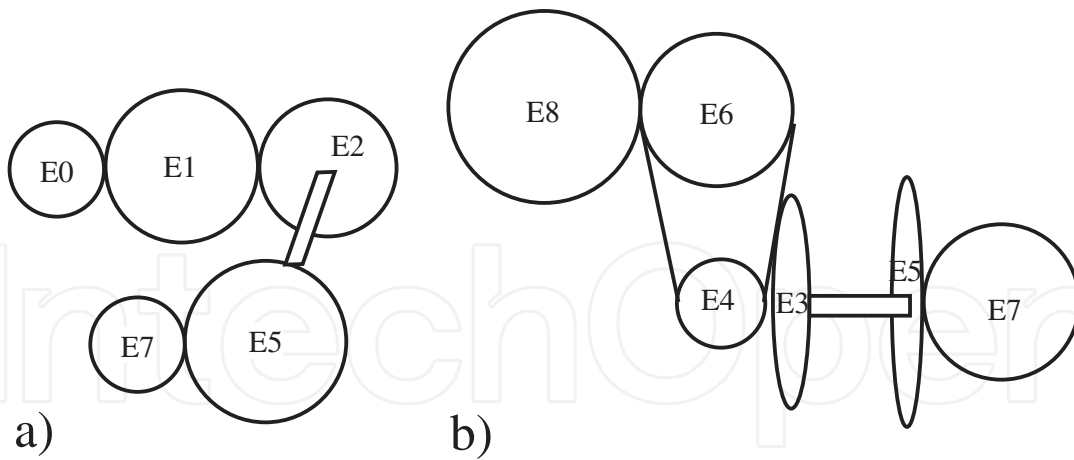
Figure 5. Steering mechanisms. (a) Goal-direction system and (b) evasive compass gearing.

$$\dot{\varphi}_1 = -\frac{r_0}{r_1}\dot{\varphi}_0; \tag{9}$$

Similarly, the gear connection $E_1 - E_2$ is algebraically simplified:

$$\dot{\varphi}_2 = -\frac{r_1}{r_2}\dot{\varphi}_1 = \frac{r_0}{r_2}\dot{\varphi}_0; \tag{10}$$

The parallel connection E_5 with E_2 has the same relation:

$$\dot{\varphi}_5 = \dot{\varphi}_2 = \frac{r_0}{r_2}\dot{\varphi}_0; \tag{11}$$

Finally, the angular velocity for E_7 w.r.t. E_0

$$\dot{\varphi}_7 = -\frac{r_5}{r_7}\dot{\varphi}_5 = -\frac{r_0 r_5}{r_2 r_7}\dot{\varphi}_0. \tag{12}$$

Thus, the relation (12) means that E_7 poses opposite rotary movement w.r.t. the absolute compass sense of rotation and half of its angular speed as well.

2.2. Local evasive compass

Another compass mechanism with local reference frame steers the robot for obstacle avoidance leading the robot along a safe instantaneous angle (**Figure 5b**). When the robot detects near obstacles, the absolute compass is suspended, and a commutator device switches to the evasive local compass mechanism, activating the gear E_8. **Figure 5b** describes the gearing mechanism that steers the robot for evasive navigation.

In the kinematic model for evasive steering through E_7, w.r.t. E_8 is deduced next. The relation between E_8 and E_6 is

$$\dot{\varphi}_6 = -\frac{r_8}{r_6}\dot{\varphi}_8; \tag{13}$$

and the angular velocity for E_4 is

$$\dot{\varphi}_4 = \frac{r_6}{r_4}\dot{\varphi}_6 = -\frac{r_8}{r_4}\dot{\varphi}_8, \tag{14}$$

For the perpendicular connection with E_3, the angular speed model is

$$\dot{\varphi}_3 = -\frac{r_4}{r_3}\dot{\varphi}_4 = \frac{r_8}{r_3}\dot{\varphi}_8; \tag{15}$$

For E_3 and E_5 connected in parallel

$$\dot{\varphi}_5 = \dot{\varphi}_3 = \frac{r_8}{r_3}\dot{\varphi}_8; \tag{16}$$

Finally, the model for E_7 is

$$\dot{\varphi}_7 = -\frac{r_5}{r_7}\dot{\varphi}_5 = -\frac{r_8 r_5}{r_2 r_7}\dot{\varphi}_8. \tag{17}$$

Let us highlight that for the evasive local compass E_8, the escaping orientation is instantaneously set up by an actuator only when any nearby obstacle is detected. And, such local orientation transmits motion to the steering gear (E_7) through the mechanism of **Figure 5b**. Thus, the local/global compass mechanisms are physical controllers that substitute models and computer algorithms.

## 3. Absolute/local commuting mechanism

The commutation mechanism interactively couples and uncouples either the absolute compass or the local compass (**Figure 6a**). The commuting device switches into the local compass immediately where any nearby obstacle is detected. Alternatively, it switches to the global compass retaking orientation toward the goal as soon as obstacles are no longer detected. **Figure 7a** depicts the gearing transmission that commutates the different steering mechanisms, the local compass (the front), and the global compass (the back).

According to **Figure 6b**, the commutation mechanism yields linear motion (the commutator device of **Figure 6a**); it activates the local compass by rotating a servomotor and shrinking a sliding crank link L. Inversely, the absolute compass is activated by turning off the servomotor, and then a spring-mass-damper system stretches the sliding crank link L.

The motion transmission system (**Figure 6a**) is inspired by the model of a modern vehicle's speed transmission box. For the present case, a common shaft works for two asynchronous speed gearing systems. In addition, **Figure 7a** and **7b** illustrates the motion transmission flow
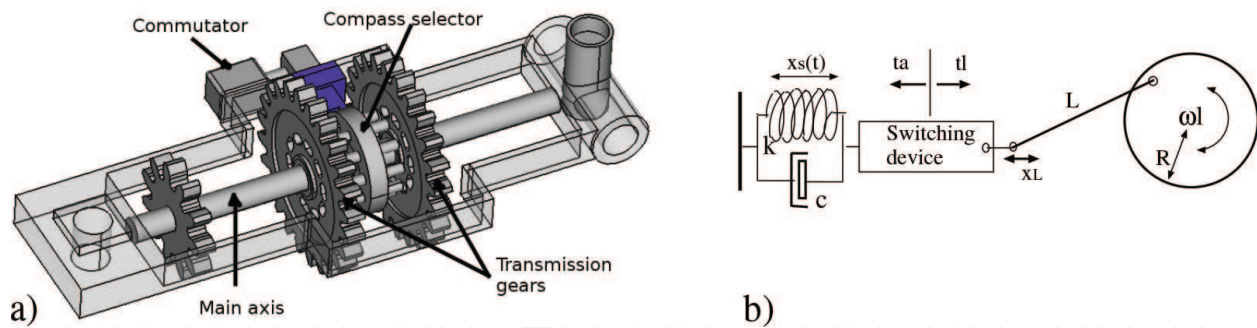
Figure 6. Commutator device. (a) Absolute/evasive motion transmission system and (b) basic commuter mechanism.
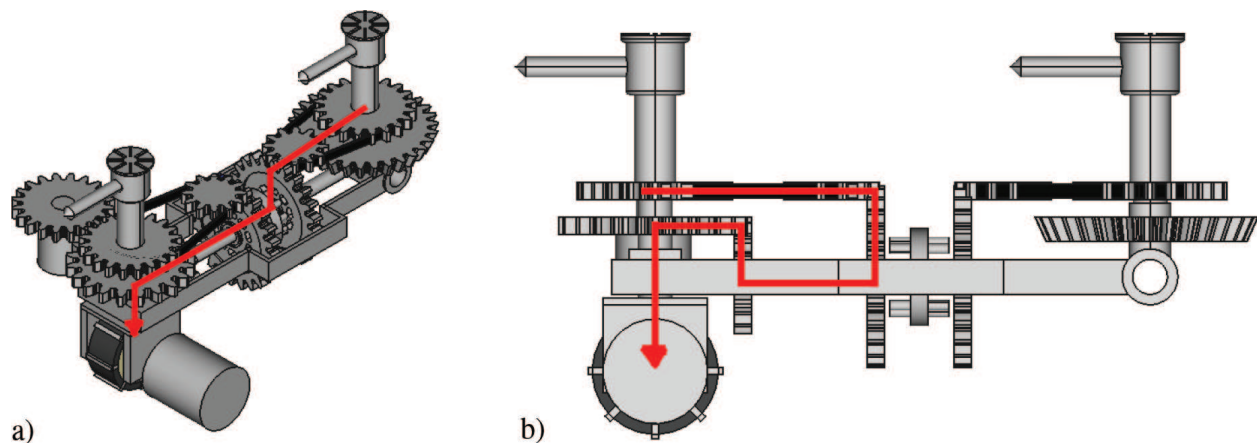
Figure 7. Motion transmission flow (red arrowed lines). (a) Goal-reference and (b) obstacle evasive.

by the red color arrowed lines. When either the local compass mechanism or the global compass mechanism is commutated, the flow transmission motion only concerns with its own gearing mechanism featuring a physical continuous controller.

The angular speed model ω_l [s^{-1}] for the commutation rotary servomotor (**Figure 6b**) to switch into the local compass was obtained through fitting empirical observations with the next theoretical model:

$$\omega_l = \kappa_1 e^{\kappa_2 t};$$

(18)

where κ_1 [rad/s] is an amplitude factor and κ_2 [1/s] is a slope rate factor. Subsequently, to estimate the commutation time t_l [s] required to mechanically coupling into the local compass mechanisms, the next model is deduced:

$$t_l = \frac{\ln\left(\frac{\omega_l}{\kappa_2}\right)}{\kappa_1}.$$

(19)

Moreover, when no obstacles are detected, the commuter device switches into its initial state by coupling the absolute compass. In this case, an underactuated system commutates the state by a spring-mass-damper mechanical system with critically dumped configuration, modeled

by second-order linear differential equation. Where m [kg] is the mass pulling the spring, c [kg/s] is the damping effect constant, k [kg/s^2] is the spring elasticity constant, and x, $\dot{x}$, and $\ddot{x}$ are the spring distance, velocity, and acceleration, respectively:

$$m\ddot{x} + c\dot{x} + kx = 0 \tag{20}$$

Thus, it may be solved as a first-order linear equation by temporally omitting the second-order term $m\ddot{x}$ such that

$$c\frac{dx}{dt} = -kx, \tag{21}$$

reorganizing and completing the integrals

$$\int_x \frac{dx}{x} = \frac{-k}{c}\int_t dt, \tag{22}$$

Thus, by solving the improper integrals and multiplying both sides of the equation by the Euler number e,

$$e\left[\ln(x) = -\frac{k}{c}t + C_1\right] \tag{23}$$

and a solution is obtained; to simplify let us define $\lambda := -k/c$,

$$x(t) = e^{\lambda t + c_1} \tag{24}$$

Assuming the integration constant $C_1 = 0$ and developing the higher order solutions

$$x(t) = e^{\lambda t}; \quad \dot{x}(t) = \lambda e^{\lambda t}; \quad \ddot{x}(t) = \lambda^2 e^{\lambda t}. \tag{25}$$

In addition, by substituting such functions in the next expression

$$m\lambda^2 e^{\lambda t} + c\lambda e^{\lambda t} + ke^{\lambda t} = 0, \tag{26}$$

In order to decrease the commutation time of the sliding linear mechanism, a critically damped system is assumed and modeled by $(c^2 - 4mk) = 0$, with terms $\lambda_1 = \lambda_2$:

$$\lambda_{1,2} = \frac{-c}{2m}, \tag{27}$$

It is desired to speed up as much as possible the commutation time. Then, the mechanical device linear displacement is modeled as a function of time by

$$x(t) = (a_1 + a_2)e^{-ct/2m}. \tag{28}$$

And, solving for the commutation time for switching to the absolute compass t_a,
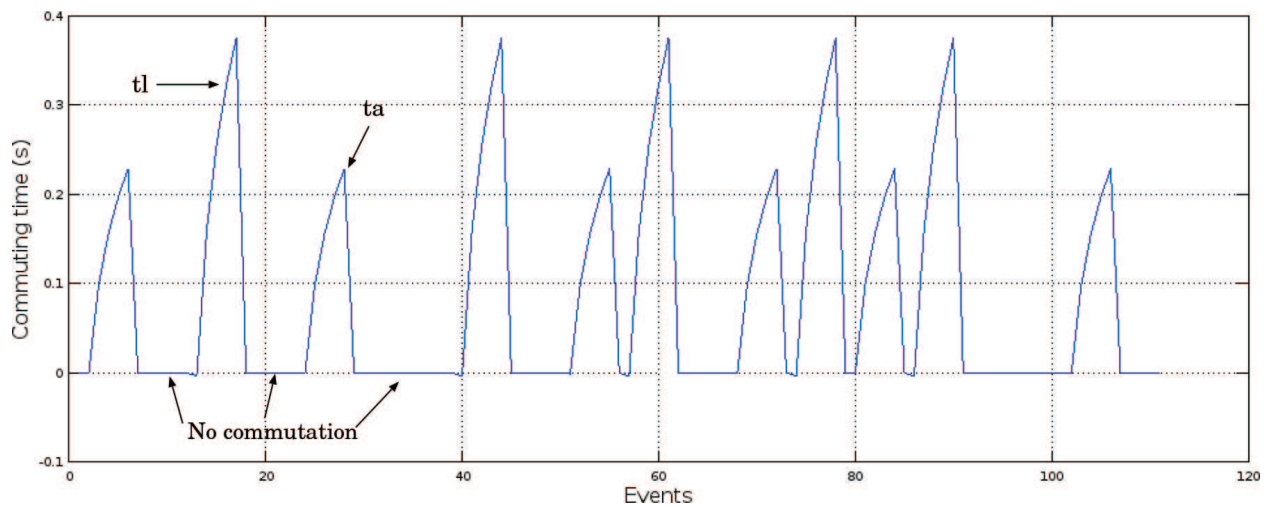
Figure 8. Commuting times: t_a (absolute mechanism) and t_l (local mechanism).

$$t_a = -\frac{2m}{c} \ln \left(\frac{x}{a_1 + a_2} \right) \tag{29}$$

Figure 8 depicts a sequence of transition times taken by the commuting mechanism. Times t_l are the times behavior of the slider crank servomotor when shrinking the link. Times t_a are the times behavior of the spring-mass-damper device when stretching the link. Such time magnitudes are reached due to mechanical motions. However, such commutation times are physically fast enough, and a robot's trajectory is not affected in the precise points when commutations occur.

4. Kinematic control law

In this section, a kinematic control law is deduced and analyzed. The proposed controller simultaneously controls driving and self-steering velocities and keeps track of the robot's posture. The robotic platform is a tricycle-type kinematic structure with two lateral passive wheels at the back (**Figure 9a**) and a central active-drive and passive self-steering wheel at the front (**Figure 9b**). Each wheel kinematic is described by three parameters, α, ℓ, and r, where α [rad] is the angle of a wheel w.r.t. the x-axis of the robot's fixed inertial system, ℓ [m] is the distance between the robot's centroid and each wheel's contact point with the ground, and r [m] is an ideal wheel's radius. In addition, the robot's kinematic structure considers two controlled kinematic variables β_t and φ_t, where β_t [rad] is the instantaneous steering angle of the front-sided wheel and φ [rad] is the instantaneous driving wheel's angle.

The kinematic parameters and variables describing the robot platform are summarized in **Table 1** according to each type of wheel (fixed passive, steerable, and drivable active).

The robot's wheel kinematic parameter is modeled by the following constraint equation, which is stated from the wheel plane,
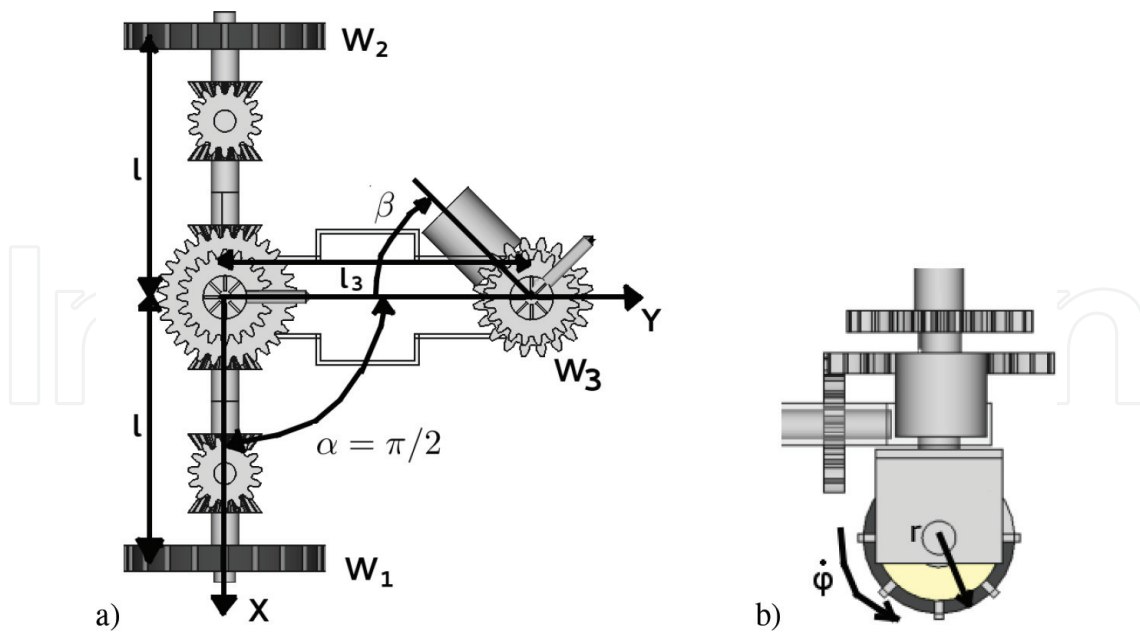
Figure 9. Robot's kinematic structure. (a) Top-view kinematic structure and (b) side-view drive-steer wheel.

Wheel type	α	β_t	ℓ
W_1 (fixed)	0	0	ℓ
W_2 (fixed)	π	0	ℓ
W_3 (drive/steer)	$\pi/2$	—	ℓ_3

Table 1. Tricycle-type robot's wheel kinematic parameters and variables.

$$\mathbf{J}_1(\beta_t)\mathbf{R}(\theta_t)\dot{\xi}_t + \mathbf{J}_2\varphi_t = 0, \tag{30}$$

Likewise, the kinematic constraint is modeled in the wheel's orthogonal plane by

$$\mathbf{C}_1(\beta_T)\mathbf{R}(\theta_t)\dot{\xi}_t = 0. \tag{31}$$

where $\mathbf{J}_1, \mathbf{C}_1 \in \mathbb{R}^{N \times 3}$ basically describes the wheel kinematic constraints. Matrix $\mathbf{J}_2$ poses the ideal wheel's radius, and $\mathbf{R}(\theta)$ is the Euler rotation matrix. Vector ξ_t describes the state space system, and its components are the robot's posture $\xi = (x, y, \theta, \beta)^\mathrm{T}$, as well as the front-sided wheel driving speed φ_t, and its product with $\mathbf{J}_2$ establishes a diagonal matrix of the wheels' tangential velocities.

Moreover, for the particular case of fixed wheels and central orientable wheels, the following kinematic constraints apply for individual wheels.

In the wheel's plane

$$\left[-\sin(\alpha + \beta_t) \quad \cos(\alpha + \beta_t) \quad \ell\cos(\beta_t) \right] \cdot \mathbf{R}(\theta_t) \cdot \dot{\xi}_t + r\dot{\varphi}_t = 0. \tag{32}$$

In the wheel's orthogonal plane

$$\left[\; \cos\left(\alpha + \beta_t\right) \quad \sin\left(\alpha + \beta_t\right) \quad \ell\sin\left(\beta_t\right)\;\right] \cdot \mathbf{R}(\theta_t)\dot{\boldsymbol{\xi}}_t = 0. \tag{33}$$

where matrix $\mathbf{J}_1$ is the fixed passive back-sided wheels matrix of kinematic constraints, which is obtained by substituting the parameters of **Table 1** in expression (32). Such that, $\mathbf{J}_f$ for the fixed wheels is

$$\mathbf{J}_f = \begin{pmatrix} -\sin\left(0\right) & \cos\left(0\right) & \ell\cos\left(0\right) \\ -\sin\left(\pi\right) & \cos\left(\pi\right) & \ell\cos\left(0\right) \end{pmatrix}, \tag{34}$$

and by simplifying

$$\mathbf{J}_f = \begin{pmatrix} 0 & 1 & \ell \\ 0 & -1 & \ell \end{pmatrix}. \tag{35}$$

Taking into account the kinematic constraints that are similar to the central orientable wheel, the vector model $\mathbf{J}_o$ is obtained:

$$\mathbf{J}_o = \left(-\sin\left(\frac{\pi}{2} + \beta_t\right) \quad \cos\left(\frac{\pi}{2} + \beta_t\right) \quad \ell_3\cos\left(\beta_t\right) \right) \tag{36}$$

For the front-sided central orientable wheel, since the angle β_t is nonstationary, and in order to easy its algebraic solution the following trigonometric identities are substituted in (36) and obtain a simplified form for the vector $\mathbf{J}_o$. Thus,

$$\sin\left(a + b\right) = \sin\left(a\right)\cos\left(b\right) + \cos\left(a\right)\sin\left(b\right),$$

Likewise,

$$\cos\left(a + b\right) = \cos\left(a\right)\cos\left(b\right) - \sin\left(a\right)\sin\left(b\right);$$

and the following row vector is produced:

$$\mathbf{J}_o = \left(-\cos\left(\beta_t\right) \quad -\sin\left(\beta_t\right) \quad \ell_3\cos\left(\beta_t\right) \right). \tag{37}$$

Therefore, for a tricycle-type robotic structure as in the present context, and with parameters of **Table 1**, the matrix $\mathbf{J}_1$ is consequently defined as

$$\mathbf{J}_1 = \begin{pmatrix} \mathbf{J}_f \\ \mathbf{J}_o \end{pmatrix} = \begin{pmatrix} 0 & 1 & \ell \\ 0 & -1 & \ell \\ -\cos\left(\beta_t\right) & -\sin\left(\beta_t\right) & \ell_3\cos\left(\beta_t\right) \end{pmatrix}, \tag{38}$$

where $\mathbf{J}_f$ represents the fixed wheel kinematic constraints and $\mathbf{J}_o$ represents the central orientable wheel constraints. The constraints denoted in the general form (31) implicate that vector $\mathbf{R}(\theta_t) \cdot \dot{\boldsymbol{\xi}}_t$ belongs to the null space $\mathbf{C}_1^*$ denoted by

$$\mathbf{C}_1^*(\beta_t) = \begin{pmatrix} \mathbf{C}_f \\ \mathbf{C}_\beta \end{pmatrix} \tag{39}$$

being $\mathbf{C}_f$ and $\mathbf{C}_\beta$ as vectors of the fixed and the central orientable wheel constraint, respectively, with notation

$$\mathbf{R}(\theta_t) \cdot \dot{\xi}_t \in \mathcal{N}\left[\mathbf{C}_1^*(\beta_t)\right]. \tag{40}$$

Hence, the robot's posture first-order derivative $\dot{\xi}(t)$ or state vector is constrained into a distribution defined as

$$\mathcal{N}\left[\mathbf{C}_1^*(\beta)\right] = \text{span}\{\text{col}\Sigma(\beta)\}, \tag{41}$$

and the null space of any matrix $\mathbf{A}$, written as a $\mathcal{N}(\mathbf{A})$, is the set of all solutions of $\mathbf{A} \cdot \mathbf{x} = 0$ and stated in set notation by

$$\mathcal{N}(\mathbf{A}) = \{\mathbf{x} \in \mathbb{R}^x | \mathbf{A} \cdot \mathbf{x} = 0\}. \tag{42}$$

Thus, for the particular case of Eq. (41), the null space is

$$\mathcal{N}\left[\mathbf{C}_1^*(\beta_t)\right] = \{\mathbf{x} \in \mathbb{R}^3 | [C_1^*(\beta_t)]\mathbf{x} = 0\}. \tag{43}$$

A manner to solve for the null space matrix condition is to reduce it to the echelon form Ψ:

$$\mathbf{C}_1 = \begin{pmatrix} 1 & 0 & 0 \\ -1 & 0 & 0 \\ -\sin(\beta_t) & \cos(\beta_t) & \ell_3 \sin(\beta_t) \end{pmatrix}, \tag{44}$$

Thus, a vector $\mathbf{x}$ that satisfies Eq. (43) must be defined then:

$$\begin{pmatrix} 1 & 0 & 0 \\ -1 & 0 & 0 \\ -\sin(\beta_t) & \cos(\beta_t) & \ell_3 \sin(\beta_t) \end{pmatrix} \cdot \begin{pmatrix} x_1 \\ x_2 \\ x_3 \end{pmatrix} = \begin{pmatrix} 0 \\ 0 \\ 0 \end{pmatrix}. \tag{45}$$

The previous expression (45) is a set of linear systems and is rewritten as an augmented matrix $[\mathbf{C}_1 | \mathbf{0}]$:

$$[\mathbf{C}_1|\mathbf{0}] = \begin{pmatrix} 1 & 0 & 0 & | & 0 \\ -1 & 0 & 0 & | & 0 \\ -\sin(\beta) & \cos(\beta) & \ell_3 \sin\beta & | & 0 \end{pmatrix}. \tag{46}$$

The augmented matrix (46) is algebraically solved by reducing it to echelon form, starting by making zeros the first column, but one the first element:

$$\Psi = \begin{pmatrix} 1 & 0 & 0 \\ 0 & 0 & 0 \\ -\sin(\beta_t) & \cos(\beta_t) & \ell_3 \sin(\beta_t) \end{pmatrix}, \tag{47}$$

Then, sum up $\Psi_{1,i} \Psi_{3,1}$ where $\Psi_{3,1} = \sin(\beta_t)$:

$$\Psi = \begin{pmatrix} 1 & 0 & 0 \\ 0 & 0 & 0 \\ 0 & \cos(\beta_t) & \ell_3 \sin(\beta_t) \end{pmatrix}. \tag{48}$$

Since the pivot element $\Psi_{2,2} = 0$, rows 2 and 3 are exchanged:

$$\Psi = \begin{pmatrix} 1 & 0 & 0 \\ 0 & \cos(\beta_t) & \ell_3 \sin(\beta_t) \\ 0 & 0 & 0 \end{pmatrix}. \tag{49}$$

Now, $\Psi_{i,2} = \mathbf{0}$ except its pivot element $\Psi_{2,2}$, thus let us divide $\Psi_{2,i}/\cos(\beta_t)$ to set to 1 such pivoting element:

$$\Psi = \begin{pmatrix} 1 & 0 & 0 \\ 0 & 1 & \ell_3 \tan(\beta_t) \\ 0 & 0 & 0 \end{pmatrix}. \tag{50}$$

Thus, by having Ψ in the reduced form, now the system is solved as the system (45):

$$\begin{pmatrix} 1 & 0 & 0 \\ 0 & 1 & \ell_3 \tan(\beta_t) \\ 0 & 0 & 0 \end{pmatrix} \cdot \begin{pmatrix} x_1 \\ x_2 \\ x_3 \end{pmatrix} = \begin{pmatrix} 0 \\ 0 \\ 0 \end{pmatrix}. \tag{51}$$

Hence, rewriting such a solution in the matrix form

$$\mathbf{x} = \begin{pmatrix} 0 \\ -\ell_3 \tan(\beta) \\ 1 \end{pmatrix} x_3 \tag{52}$$

Being the vector $\mathbf{x}$ of this null space of matrix $\mathbf{C}_1$, such that

$$\mathcal{N}\left[\mathbf{C}_1^*(\beta)\right] = \text{span} \begin{pmatrix} 0 \\ -\ell_3 \tan(\beta) \\ 1 \end{pmatrix} x_3; \tag{53}$$

For our application purpose, $x_3 = \cos\beta$, then the null space solution $\mathcal{N}\left[\mathbf{C}_1^*(\beta)\right]$ is

$$\mathcal{N}\left[\mathbf{C}_1^*(\beta)\right] = \text{span} \begin{pmatrix} 0 \\ -\ell_3 \sin\beta \\ \cos\beta \end{pmatrix}. \tag{54}$$

Therefore, Eq. (41) is rewritten because for each instant time t, a temporal variable v_t exist .

$$\dot{\xi} = \mathbf{R}^{\mathrm{T}}(\theta_t)\mathbf{\Sigma}(\beta_t)v_t, \tag{55}$$

and

$$\dot{\beta}_t = w_t. \tag{56}$$

where v_t is the instantaneous robot's absolute velocity and w_t is instantaneous robot's yaw rate. As a matter of fact $\mathbf{\Sigma}(\beta_t)$ is the null space of the kinematic constraint matrix in the wheel's orthogonal plane (Eq. (54)), defined by

$$\mathbf{\Sigma}(\beta_t) = \begin{pmatrix} 0 \\ -\ell_3 \sin(\beta_t) \\ \cos(\beta) \end{pmatrix}. \tag{57}$$

This state control law is expressed in a more compact form:

$$\dot{\mathbf{z}}_t = \mathbf{B}(z)\mathbf{u}_t; \tag{58}$$

where

$$\mathbf{z} = \begin{pmatrix} \xi_t \\ \beta_t \end{pmatrix}; \quad \mathbf{B}(z_t) = \begin{pmatrix} \mathbf{R}^{\mathrm{T}}(\theta_t)\mathbf{\Sigma}(\beta_t) & 0 \\ 0 & 1 \end{pmatrix}; \quad \mathbf{u} = \begin{pmatrix} v \\ w \end{pmatrix}. \tag{59}$$

Thus, by substituting expression (57) in the model (58), the kinematic control law is rewritten:

$$\begin{pmatrix} \dot{x} \\ \dot{y} \\ \dot{\theta} \\ \dot{\beta} \end{pmatrix} = \begin{pmatrix} \ell_3 \sin\theta \, \sin\beta & 0 \\ -\ell_3 \cos\theta \, \sin\beta & 0 \\ \cos\beta & 0 \\ 0 & 1 \end{pmatrix} \cdot \begin{pmatrix} v \\ w \end{pmatrix}. \tag{60}$$

The robot's posture is essentially modeled by Eq. (60) and validates by the Cartesian trajectory depicted in **Figure 10a**. For this case, v was set at constant value overtime, and w gradually increased according to the range $\{0, \ldots, \pi/4\}$. Then, the robot turns into its original angle and then continues straight.

Figure 10b and **10c** shows β and θ behaviors w.r.t. orientation error θ_E, when $\theta_E = 0$ the robot is bearing toward the desired goal. Actually, β depicts how the steering wheel performs from its starting angle up to the final angle. Because of the absence of obstacles, the steering wheel's angle experiences no commutation toward the local mechanism. However, the absolute compass controls the wheel from the beginning and gradually steers until orientation is aligned to the global destination. Its behavior along the navigation task is illustrated in plot 10b.

Moreover, in order to instantaneously estimate the deviation angle θ_E, let us define the global destination θ_G [rad]. And, such desired orientation is perturbed by escaping angle θ_R [rad] due to relative obstacle locations (**Figure 11a**). Likewise, θ_R is established every time the local compass mechanism is switched to. Obstacles are detected within a territorial radius d_l, or ignored when the robot moves farther away from the scope d_l (**Figure 11b**).
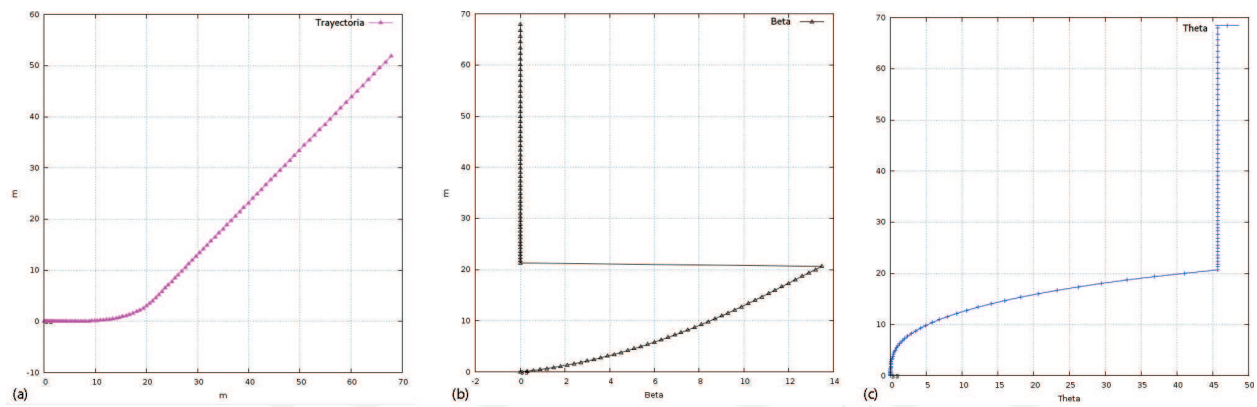
Figure 10. Control law (60) simulation results. (a) Trajectory control with v=cte and w ranging $\beta = \{0, \ldots, \pi/4\}$, (b) wheel's steer angle β behavior, and (c) robot's angle θ behavior.
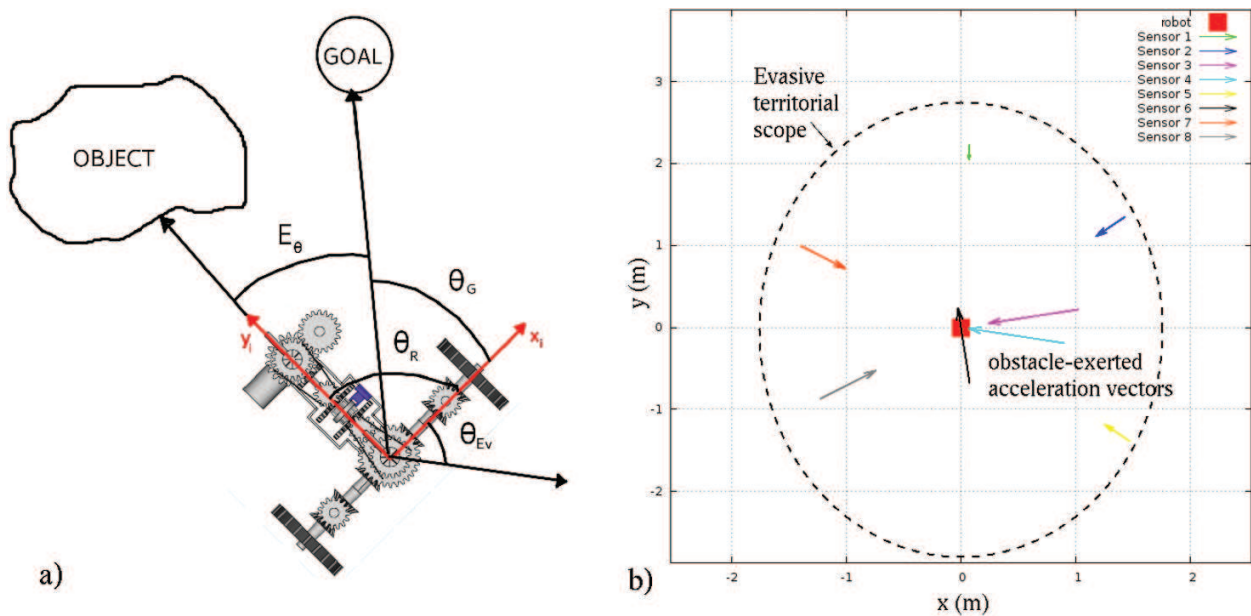
Figure 11. Evasive system. (a) θ_R and θ_G kinematics and (b) evasive territorial scope and obstacle-repulsive acceleration vectors.

For instance, sensor 1 detects a far obstacle, and its repulsive acceleration influence is low. However, sensor 6 yields a greater repulsive acceleration influence since it is nearer to the robot's location.

Thus, let us postulate:

$$\theta_E = \theta_R - \theta_G \tag{61}$$

From the control law, the state vector **z** is now estimated by directly using the instantaneous error angle θ_E:

$$\dot{\mathbf{z}}(\dot{x}, \dot{y}, \theta_E, \beta) = \mathbf{B}(z) \cdot \mathbf{u}(v, w), \tag{62}$$

and by obtaining the inverse solution for **u**, now the input system involves error angle:

$$\mathbf{u}(v, w) = \mathbf{B}(z)^{-1} \cdot \dot{\mathbf{z}}\left(\dot{x}, \dot{y}, (\theta_R - \theta_G), \beta\right). \tag{63}$$

The robot's controlled orientation is fed back by θ_E and calculated by numerical successive approximations. This controller is a recursive system that involves both, the direct and the inverse solutions, to reduce the numerical error θ_E.

The instantaneous escaping angle θ_R is obtained within a local coordinate system by directional derivatives, which approach a cosine function, similarly to the work reported in Ref. [20]. A gradient operator of a cosine navigation function approximates a repulsive partial differential equation to evade any observable obstacle. The robot's repulsive acceleration vector function $\mathfrak{a}_\alpha = \left(a_x, a_y\right)^\top$ produces its magnitude effect w.r.t. the obstacle's range measurement δ_α [m]:

$$\mathfrak{a}_\alpha(x, y) = -\nabla_{x,y} k_\alpha (k_2 - r_\alpha) \cdot \cos\left(\phi_\alpha\right) \tag{64}$$

where k_2 [m] is the obstacle diametrical territory and k_α [ms^{-2}] is an adjustment constant factor of the physical acceleration amplitude. Thus, the Cartesian geometric model (not measurement) r_α describes the distance between the robot $\mathbf{x}_r = (x_r, y_r)^\top$ and any obstacle $\mathbf{x}_o = (x_o, y_o)^\top$, which is geometrically modeled by

$$r_\alpha = \sqrt{x^2 + y^2} = \sqrt{(x_r - x_o)^2 + \left(y_r - y_o\right)^2} \tag{65}$$

The angle limits $\{0 \leq \phi_\alpha \leq \pi/2\}$ is a transformation relationship of the obstacle range δ_α, and the condition $\delta_\alpha < d_l$ limits the repulsive acceleration effects:

$$\phi_\alpha = \frac{\delta_\alpha \pi}{2 d_l}; \quad \text{where } d_l \propto \frac{\pi}{2} \text{ and } d_l = \delta_\alpha \Rightarrow \|\mathfrak{a}\| = 0 \tag{66}$$

Substituting the functional form of δ_α in (64) and temporally considering $k_\alpha = 1$ for analysis purpose

$$\mathfrak{a}_\alpha(x, y) = -\nabla_{x,y}\left(\left(k_2 - \sqrt{(x_r - x_o)^2 + \left(y_r - y_o\right)^2}\right) \cdot \cos\left(\phi_\alpha\right)\right) \tag{67}$$

and algebraically expanding

$$\mathfrak{a}_\alpha(x, y) = -\nabla_{x,y}\left(-k_2 \cos\left(\phi_\alpha\right) + \sqrt{(x_r - x_o)^2 + \left(y_r - y_o\right)^2} \cdot \cos\left(\phi_\alpha\right)\right) \tag{68}$$

Thus, applying the gradient operator $\nabla_{x,y}$ w.r.t. x and y components and algebraically simplifying

$$\frac{\partial \mathfrak{a}_\alpha}{\partial x} = \frac{(x_r - x_o) \cdot \cos\left(\phi_\alpha\right)}{\sqrt{(x_r - x_o)^2 + \left(y_r - y_o\right)^2}} \tag{69}$$

and

$$\frac{\partial \mathfrak{a}_\alpha}{\partial y} = \frac{\left(y_r - y_o\right) \cdot \cos\left(\phi_\alpha\right)}{\sqrt{(x_r - x_o)^2 + \left(y_r - y_o\right)^2}} \tag{70}$$

Therefore, the obstacle-repulsive directional vector expressed in terms of Cartesian components XY is

$$\mathfrak{a}_\alpha(x, y) = k_\alpha \frac{\cos(\phi_\alpha)}{\sqrt{(x_r - x_o)^2 + (y_r - y_o)^2}} \cdot \begin{pmatrix} x_r - x_o \\ y_r - y_o \end{pmatrix} \tag{71}$$

Thus, the model for multiple obstacles α produces a controlled escaping direction in robot's local coordinate framework:

$$\mathbf{a}_T = k_\alpha \sum_\alpha \frac{\cos(\phi_\alpha)}{\sqrt{(x_r - x_o)^2 + (y_r - y_o)^2}} \cdot \begin{pmatrix} x_r - x_o \\ y_r - y_o \end{pmatrix} \tag{72}$$

It follows that the evasive acceleration magnitude is defined by

$$\|\mathbf{a}_T\| = \sqrt[2]{\left(\frac{\partial \mathfrak{a}_\alpha}{\partial x}\right)^2 + \left(\frac{\partial \mathfrak{a}_\alpha}{\partial y}\right)^2}, \tag{73}$$

and the instantaneous escaping angle θ_R

$$\theta_R = \arctan\left(\frac{\left(\frac{\partial a}{\partial y}\right)}{\left(\frac{\partial a}{\partial x}\right)}\right). \tag{74}$$

Finally, the proposed kinematic controller has the following scheme described in Algorithm 1.

**Algorithm 1.** Local/global robot's underactuated system controller

---

1 $\omega_l = 0.0$
2 while $(\|\xi_t\| - \|(x_G, y_G)\|) > 0$ **do**
3   switching to either local or global mechanism
4   **if** $\delta_\alpha > 0$
5   Commuter's motor speed $\omega_l = k_1 e^{k_2 t}$
6   Servo's angle $\phi = \frac{\omega_l \kappa_1}{\ln\left(\frac{\omega_l}{\kappa_2}\right)}$
7   Avoidance acceleration $\mathbf{a}_T = k_\alpha \sum_\alpha \frac{\cos(\phi_\alpha)}{r_\alpha}(\mathbf{x}_r - \mathbf{x}_\alpha)$
8   Avoidance angle $\theta_R = \arctan\left(\frac{\partial a/\partial y}{\partial a/\partial x}\right)$
9 $\|\mathbf{a}_T\| = \sqrt[2]{(\partial a/\partial x)^2 + (\partial a/\partial y)^2}$
10   **else**
11   Turns servo off $\omega_l = 0.0$
12   Release slider crank $x_a = r\cos(\phi)\sqrt[2]{(a_1 + a_2)^2 e^{-ct/m} - (r\sin(\phi))^2} + \Delta s$
13 $\theta_G = -\frac{\varphi_{w1} - \varphi_{w2}}{4}$
14 $\theta_E = \theta_R - \theta_G$
15 $\mathbf{u} = \left(\frac{\|\mathbf{a}_T\|}{\Delta t}, \frac{d\theta_E}{dt}\right)^T$
16 $\dot{\mathbf{z}}_t = \mathbf{B}(\theta_E, \beta) \cdot \mathbf{u}_t$
17 $\mathbf{u}_{t+1} = \mathbf{B}^{-1} \cdot \dot{\mathbf{z}}$
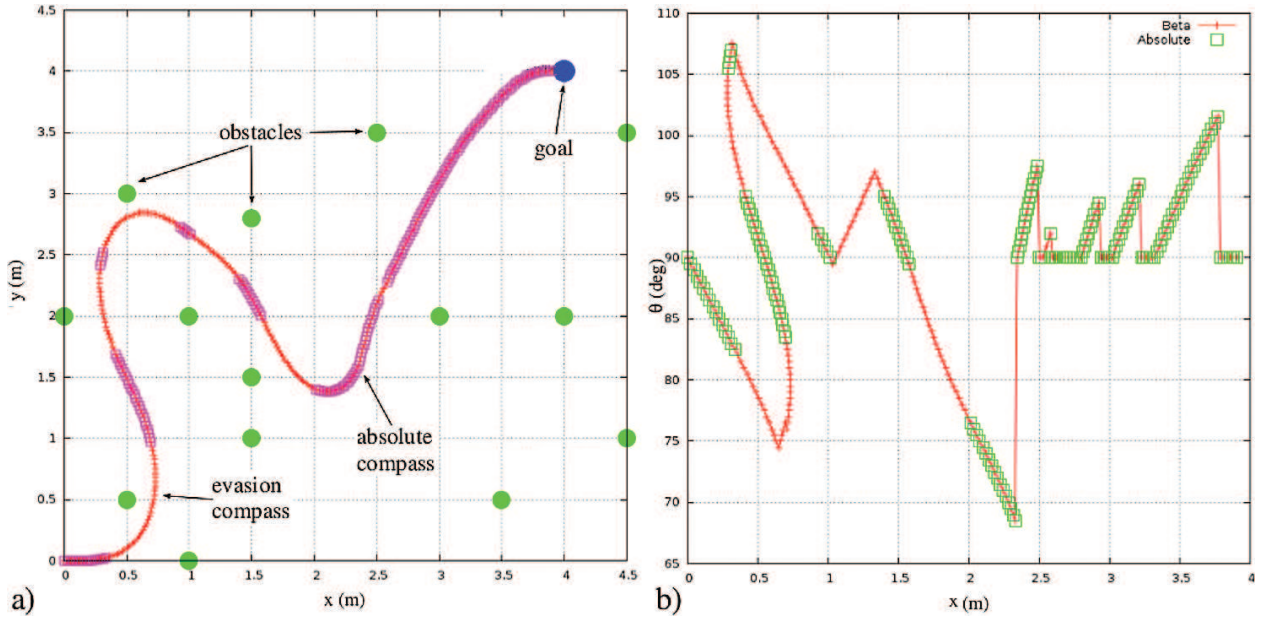
Figure 12. Controlled robot's course $v = 1.0$ *rad/s* and $d_l = 0.5$ *m*. (a) Cartesian space and (b) component *X* versus robot's angle.

Hereafter, **Figure 12** validates our kinematic model approach by depicting how the robot's trajectory reaches the final Cartesian goal $(-7, -8)$ in global coordinates. In addition, **Figure 12a** shows the Cartesian trajectory among multiple obstacles and the local/global commuting steering modalities. Likewise, as a manner to show validation, **Figure 12b** illustrates only the component *X* versus the robot's angle during the same navigational task.

5. Conclusion

The interest of this chapter was to introduce the analysis of an alternative kinematic steering controller by using underactuated mechanical compasses and to demonstrate its feasibility, controllability approach, and natural efficiency. Despite the complexity in its implementation, a compass mechanism is proposed because it allows to directly set up the global goal as an absolute reference. Moreover, the compass mechanism itself directly steers the robot to the goal simultaneously avoiding obstacles. These functional features are important advantages for a robotic platform w.r.t. other traditional orientation systems, because the global orientation depends neither on feedback from sensor devices nor on computational complexity expenses to instantaneously estimate the global destination orientation. Unlike kinematic redundant structures, the proposed approach limits electric energy use for one driving actuator, not for steering actuators. Steering controllers no longer spend algorithmic computational resources, reserving such resources either for other robotic algorithmic tasks or for increasing additional hardware devices. Mechanical controllers are slow if compared with software algorithms, even though mechanisms are fast enough w.r.t. the available robot's mobility speeds. In this regard, a critical issue is the commutation linear actuator, which is passive/ active based on a slider crank combined with a spring-mass-damper system. The commutator device was fast enough, proving that sophisticated active linear actuators were not needed. It

was found out that commutation times between local/global compasses did not negatively affect the system performance or the trajectory stability. Local/global compasses commuting activity warranted the robot to reach the global destination while avoiding collisions. The controlled trajectories yielded were concatenations of inter-switching segments with no discontinuities found. We concluded that from the implementation perspective, the proposed approach is neither necessarily better nor worst in effectiveness than a traditional redundantly actuated and multisensor approach. As a matter of fact, a traditional approach is easier to physically implement. Nevertheless, a redundant traditional approach is in disadvantage, if driving wheels grow in number, not to mention incrementing steering actuators. As a consequence, the more redundant is a system, the more discretized are the controlled motions and trajectories lose stability, which is an inherent difference from the naturally continuous motions produced by underactuated systems. A compact linear kinematic control law to switch inter-compass usage was deduced, with direct and inverse solutions. It elegantly combined the underactuated mechanism control with a very short algorithm to detect obstacles and to estimate the instantaneous escaping orientation. It was found that the robot's trajectory continuity may be altered, if kinematic evasion parameters are readjusted consequently changing the mechanism commutation response. Through simulation results, the inter-mechanism interactions and functions were validated. For the specific case of the proposed kinematic structure, the local/global compass showed as much efficiency as any similar redundant system. The future work will focus on fault recovery from slips, sliding, or collision dynamics that get the compass orientation uncalibrated. In addition, not only to further orientation analysis but also positioning sensors to supplement and improve this underactuated approach.

Author details

Jorge U. Reyes-Muñoz, Edgar A. Martínez-García*, Ricardo Rodríguez-Jorge and Rafael Torres-Córdoba

*Address all correspondence to: edmartin@uacj.mx

Laboratorio de Robótica, Institute of Engineering and Technology, Universidad Autónoma de Ciudad Juárez, Mexico

References

[1] Li SH. The South-Pointing Carriage and the Mariner's Compass. Taipei: Yee Wen Pub. Co.; 1959

[2] Lu ZM. An analysis of the ancient Chinese South-Pointing Chariot. Journal of Sichuan University. 1979;**2**:95-101

[3] Muneharu M, Satoshi K. Study of the mechanics of the South-Pointing Chariot (the South Pointing Chariot with the bevel gear type differential gear train). Transactions of the Japan Society of Mechanical Engineers. 1990;**56**(C):462-466

[4]   Hong-Sen Y. Chap. 7. South-pointing Chariots, Reconstruction Designs of Lost Ancient Chinese Machinery, vol. 3. Dordrecht: Springer; 2007

[5]   Hong-Sen Y, Chun-Wei C. A systematic approach for the structural synthesis of differential-type South Pointing chariots. JSME International Journal Series C Mechanical Systems, Machine Elements and Manufacturing. 2006;**49**((3), SI on Advanced Technology of Vibration and Sound):920-929

[6]   Santander M. The Chinese South-Seeking chariot: A simple mechanical device for visualizing curvature and parallel transport. American Association of Physics Teachers. September 1992;**60**(9)

[7]   Junmin W, Xiangyu Y, Wei L. Integration of hardware and software designs for object grasping and transportation by a mobile robot with navigation guidance via a unique bearing-alignment mechanism. IEEE/ASME Transactions on Mechatronics. 2016;**21**(1): 576-583

[8]   Al-Faiz MZ, Mahameda GE. GPS-based navigated autonomous robot. International Journal of Emerging Trends in Engineering Research. 2015;**3**(4)

[9]   Sioma A, Blok S. Finding bearing in robot navigation with the use of the Kalman filter. Solid State Phenomena. 2013;**199**:241-246

[10]   Georgiou E., Dai J.S., Luck M., The KCLBOT: A double compass self-localizing maneuverable mobile robot. ASME. International Design Engineering Technical Conference and Computers and Information in Engineering Conference, Vol.3, pp. 427–435, 2011

[11]   Chen w, Zhang T. An indoor mobile robot navigation technique using odometry and electronic compass. International Journal of Advanced Robotic Systems. May-Jun 2017:1-15

[12]   Zhenhai H. y Shengguo H., Integrated navigation system based on differential magnetic compass and GPS, International Conference on Information Engineering and Computer Science, 2009

[13]   Parhi D, Deepak B. Kinematic model of three wheeled mobile robot. Journal of Mechanical Engineering Research. 2011:307-318

[14]   Campion G, Chung W, 17 C. Springer Handbook of Robotics. In: Handbook of Robotics. Springer-Verlag Berlin Heidelberg; 2008

[15]   Morin P, Samson C. Chap. 34. Springer Handbook of Robotics. In: Handbook of Robotics. Springer-Verlag Berlin Heidelberg; 2008

[16]   Minguez J, Lamiraux F, Lamound J. Chap. 35 Springer Handbook of Robotics. In: Handbook of Robotics. Springer-Verlag Berlin Heidelberg; 2008

[17]   Martinez-Garcia EA. Numerical modelling in robotics. OmniaScience. 2015

[18]   Alonsini N.I., Low cost obstacle detection system for wheeled mobile robot. UKACC International Conference on Control, pp. 529–533, 2012

[19] Martinez-Garcia EA. Robotic DCVG Planning for Searching Flaws on Buried Pipelines. Lap Lambert Academic; 2017

[20] Castro Jiménez L, Martínez-García EA. Thermal image sensing model for robotic planning and search. Sensors. 2016;**1253**:1-27

[21] Mujahed M., Fischer D. y Mertsching B., Tangential gap flow (TGF) navigation: A new reactive obstacle avoidance approach for highly cluttered environments, Robotics and Autonomous Systems, Vol.84, pp.15–30, 2016